



Induction of significant neutralizing antibodies against SARS-CoV-2 by a highly attenuated pangolin coronavirus variant with a 104nt deletion at the 3'-UTR

Shanshan Lu, Shengdong Luo, Chang Liu, Muli Li, Xiaoping An, Mengzhe Li, Jun Hou, Huahao Fan, Panyong Mao, Yigang Tong & Lihua Song

To cite this article: Shanshan Lu, Shengdong Luo, Chang Liu, Muli Li, Xiaoping An, Mengzhe Li, Jun Hou, Huahao Fan, Panyong Mao, Yigang Tong & Lihua Song (2023) Induction of significant neutralizing antibodies against SARS-CoV-2 by a highly attenuated pangolin coronavirus variant with a 104nt deletion at the 3'-UTR, *Emerging Microbes & Infections*, 12:1, 2151383, DOI: [10.1080/22221751.2022.2151383](https://doi.org/10.1080/22221751.2022.2151383)

To link to this article: <https://doi.org/10.1080/22221751.2022.2151383>



© 2022 The Author(s). Published by Informa UK Limited, trading as Taylor & Francis Group.



[View supplementary material](#)



Published online: 18 Dec 2022.



[Submit your article to this journal](#)



Article views: 3503



[View related articles](#)



[View Crossmark data](#)



Citing articles: 1 [View citing articles](#)

RESEARCH ARTICLE



Induction of significant neutralizing antibodies against SARS-CoV-2 by a highly attenuated pangolin coronavirus variant with a 104nt deletion at the 3'-UTR

Shanshan Lu^a, Shengdong Luo^b, Chang Liu^a, Muli Li^c, Xiaoping An^a, Mengzhe Li^a, Jun Hou^b, Huahao Fan^{✉ a}, Panyong Mao^b, Yigang Tong^a and Lihua Song^{✉ a}

^aBeijing Advanced Innovation Center for Soft Matter Science and Engineering, College of Life Science and Technology, Beijing University of Chemical Technology, Beijing, People's Republic of China; ^bDepartment of Infectious Diseases, Fifth Medical Center of Chinese PLA General Hospital, Beijing, People's Republic of China; ^cDepartment of Pathology, National Cancer Center/National Clinical Research Center for Cancer/Cancer Hospital & Shenzhen Hospital, Chinese Academy of Medical Sciences and Peking Union Medical College, Shenzhen, People's Republic of China

ABSTRACT

SARS-CoV-2 related coronaviruses (SARS-CoV-2r) from Guangdong and Guangxi pangolins have been implicated in the emergence of SARS-CoV-2 and future pandemics. We previously reported the culture of a SARS-CoV-2r GX_P2V from Guangxi pangolins. Here we report the GX_P2V isolate rapidly adapted to Vero cells by acquiring two genomic mutations: an alanine to valine substitution in the nucleoprotein and a 104-nucleotide deletion in the hypervariable region (HVR) of the 3'-terminus untranslated region (3'-UTR). We further report the characterization of the GX_P2V variant (renamed GX_P2V(short_3UTR)) in *in vitro* and *in vivo* infection models. In cultured Vero, BGM and Calu-3 cells, GX_P2V(short_3UTR) had similar robust replication kinetics, and consistently produced minimum cell damage. GX_P2V(short_3UTR) infected golden hamsters and BALB/c mice but was highly attenuated. Golden hamsters infected intranasally had a short duration of productive infection in pulmonary, not extrapulmonary, tissues. These productive infections induced neutralizing antibodies against pseudoviruses of GX_P2V and SARS-CoV-2. Collectively, our data show that the GX_P2V(short_3UTR) is highly attenuated in *in vitro* and *in vivo* infection models. Attenuation of the variant is likely partially due to the 104-nt deletion in the HVR in the 3'-UTR. This study furthers our understanding of pangolin coronaviruses pathogenesis and provides novel insights for the design of live attenuated vaccines against SARS-CoV-2.

ARTICLE HISTORY Received 26 October 2022; Revised 18 November 2022; Accepted 18 November 2022

KEYWORDS Coronavirus; SARS-CoV-2; pangolin coronavirus; neutralizing antibody; live attenuated vaccine

Introduction

The COVID-19 pandemic caused by SARS-CoV-2 (severe acute respiratory syndrome coronavirus 2) is producing unprecedented damages around the globe [1–3]. As of 2nd September 2022, the World Health Organization has reported over 601 million cases with over 6.4 million death cases. Investigation of the origin of the virus has not identified its direct ancestral viruses, but has led to the discovery of many SARS-CoV-2 related coronaviruses (SARS-CoV-2r) in both bats and pangolins [4–9]. Bat-derived coronaviruses found in Laos are the closest relatives of SARS-CoV-2 reported to date [10]. Despite the finding of these SARS-CoV-2r coronaviruses, very few of them have been cultured, thus their biology and pathogenicity remain largely unknown.

While bat viruses are the closest relative of SARS-CoV-2, pangolin coronaviruses likely also play an important role in the origin and evolution of SARS-CoV-2. Two SARS-CoV-2r pangolin coronaviruses GD/2019 and GX/2017 have been identified [6, 7]. The GD/2019 strain has a receptor binding domain (RBD) that shares high homology (97.4%) with that of SARS-CoV-2, which leads to the possibility that the origin of the SARS-CoV-2 RBD is a result of recombination between bat and pangolin coronaviruses [7]. The GX/2017 strain has an RBD that shares 86.8% identity with that of SARS-CoV-2 [6]. A recent study shows that the spike protein of GX/2017 has comparable binding capabilities to human ACE2 and mediating cell entry when compared to the SARS-CoV-2 spike protein [11]. Because of the

CONTACT Lihua Song ✉ songlihua@gmail.com Beijing Advanced Innovation Center for Soft Matter Science and Engineering, College of Life Science and Technology, Beijing University of Chemical Technology, Beijing, People's Republic of China; Yigang Tong ✉ tong.yigang@gmail.com Beijing Advanced Innovation Center for Soft Matter Science and Engineering, College of Life Science and Technology, Beijing University of Chemical Technology, Beijing, People's Republic of China; Panyong Mao ✉ maopy302@163.com Department of Infectious Diseases, Fifth Medical Center of Chinese PLA General Hospital, Beijing, People's Republic of China; Huahao Fan ✉ fanhuahao@mail.buct.edu.cn Beijing Advanced Innovation Center for Soft Matter Science and Engineering, College of Life Science and Technology, Beijing University of Chemical Technology, Beijing, People's Republic of China
✉ Supplemental data for this article can be accessed online at <https://doi.org/10.1080/22221751.2022.2151383>.

© 2022 The Author(s). Published by Informa UK Limited, trading as Taylor & Francis Group.

This is an Open Access article distributed under the terms of the Creative Commons Attribution License (<http://creativecommons.org/licenses/by/4.0/>), which permits unrestricted use, distribution, and reproduction in any medium, provided the original work is properly cited.

high similarity of RBDs of pangolin CoVs binding to ACE2 receptors between humans and pangolins, pangolin coronaviruses likely provide a repertoire of CoVs for future pandemics.

We previously reported the culture of a pangolin coronavirus GX_P2V [6], which shares an identical spike protein with other pangolin GX/2017 strains. The genome of coronavirus GX_P2V (GenBank accession number MT072864) was determined by using RNAs from the first passage of the GX_P2V sample, not a serially passaged isolate [6]. This GX_P2V genome has 29,795 nucleotides, including ten undetermined nucleotides and two unresolved termini. Considering the similarities in genetics, cell infectivity, and host tropism between this pangolin coronavirus and SARS-CoV-2, we sought to determine the complete genome of the GX_P2V isolate and investigate its biology and pathogenicity in animal models, which may help in understanding the evolution and pathogenicity of SARS-CoV-2 related viruses.

Here, we report that, compared to the original GX_P2V sample, the GX_P2V isolate is a variant with two mutations: one nonsynonymous mutation in the final amino acid codon of the nucleoprotein gene and a 104-nucleotide deletion in the hypervariable region (HVR) of the 3'-terminus untranslated region (3'-UTR). We then describe the characterization of the growth of the GX_P2V variant (hereafter renamed GX_P2V(short_3UTR)) in three cell lines (two monkey cell lines and one human lung cell line) and two small animal models. We found that GX_P2V(short_3UTR) has the capability to infect but is highly attenuated in all five of the tested infection models. The attenuation of this pangolin coronavirus isolate is likely due to the 104-nt deletion at 3'-UTR. A short duration of productive infection in golden hamsters induced neutralizing antibodies against pseudoviruses of GX_P2V and SARS-CoV-2. This work advances our understanding of pangolin coronaviruses pathogenesis and provides important insights for the design of live attenuated vaccines against SARS-CoV-2.

Materials and methods

Experimental model and subject details

Vero, BGM and Calu-3 cells, obtained from the American Type Culture Collection (ATCC) (Manassas, USA), were grown in Roswell Park Memorial Institute (RPMI) 1640 medium (Gibco, USA) supplemented with 10% fetal bovine serum (FBS) (Gibco, USA) and 100 units/mL penicillin–streptomycin (Gibco, USA) at 37°C in 5% CO₂. Stable hACE2-293T cells were kindly provided by Pro. Zheng Zhang (Shenzhen Third People's Hospital) and were cultured in DMEM (Gibco, USA) with 10% FBS and 100 units/mL penicillin–streptomycin.

The pangolin coronavirus GX_P2V, originally cultured from the lung-intestine mixed samples of a pangolin captured in anti-smuggling operations in 2017, was passaged in Vero cells [6]. Cell supernatants were harvested and centrifugated (10,000 × g) for five minutes, then supernatants were aliquoted and stored at –80°C. Virus titres were determined by using a standard 50% tissue culture infection dose (TCID₅₀) assay.

Human serum samples were collected from healthy donors, COVID-19 patients, and vaccinees of two doses of inactivated SARS-CoV-2 vaccine BBIBP-CorV at the Fifth Medical Center of General Hospital of Chinese PLA. All participants signed informed consent forms. The blood serum samples from COVID-19 patients and vaccinees were collected at 21–28 days after symptom onset, and two weeks after receiving the second vaccination, respectively. All serum samples were stored at –80°C. This study was approved by the institutional review board of the Fifth Medical Center, General Hospital of Chinese PLA (approval number: 2020027D).

Six-week-old male hamsters, six-week-old male BALB/c and 48-week-old female BALB/c were used in this study. The procedure of animal experiments was approved by the Institutional Animal Care and Use Committee of Fifth Medical Center, General Hospital of Chinese PLA (IACUC-2018-0020).

Next-generation sequencing

The eighth passage of the pangolin coronavirus GX_P2V was partially purified from cell culture supernatants by ultra-centrifugation. Total RNAs were extracted by using the AxyPrep™ body fluid viral DNA/RNA Miniprep kit (Axygen, Cat No. AP-MN-BF-VNA-250, Hangzhou, Zhejiang, China) according to the manufacturer's instructions. Whole-genome sequencing was performed using next-generation sequencing (NGS) methodology. The cDNA libraries were constructed using a TruSeq RNA library prep kit (Illumina) according to the manufacturer's instructions and sequenced on an Illumina MiSeq system. Sequence data was deposited in the China National Microbiological Data Center (project accession number NMDC10017729 and sequence accession number: NMDC40002427).

Assembly and characterization of the coronavirus genome

Raw reads were adaptor- and quality-trimmed with the Fastp programme [12]. The clean reads were then mapped to the near complete genome of pangolin coronavirus GX_P2V (GenBank accession number MT072864) using Bowtie 2 [13]. The reads that were mapped to the GX_P2V genome were then assembled

by *de novo* using Trinity with default settings [14]. The assembled contig had a complete 3'-terminus. Then, the 5'-terminus of the viral genome was determined by 5'/3' RACE kits (TaKaRa). The resulting whole genome sequence of GX_P2V(short_3UTR) was deposited in GenBank (accession number MW532698). To characterize and map the mutations of GX_P2V (short_3UTR), the viral genomic sequences of GX_P2V(short_3UTR) and the GX_P2V sample were aligned using ClustalW [15].

Plaque assay and cytopathic effect (CPE)

The plaque assay using methylcellulose, a low-viscosity, semi-solid overlay, was performed to determine the plaque phenotype and infectious titres as previously described [16]. Confluent monolayers of BGM, Vero and Calu-3 cells seeded in 6-well plates were incubated with ten-fold serially diluted viral stocks ranging from 10^{-1} – 10^{-6} for 2 h at 37°C with gentle rocking every 15 min. After viral adsorption, cells were washed twice with phosphate buffer saline (PBS) and overlaid with Minimum Essential Medium (MEM) (Gibco, USA) containing 2% FBS, 1% methylcellulose, and HEPES (20 mM) and incubated at 37°C in 5% CO₂ incubator. Cytopathic effect (CPE) was observed and photographed daily for 5 days under a light microscopy. At 5 days post-infection (d.p.i.), cells were fixed with 4% paraformaldehyde for 2 h at room temperature, and then stained with 0.2% crystal violet for 20 min. They were gently rinsed under tap water and dried prior to analysis of the plaque phenotype and calculation of virus titres.

Viral growth kinetics

Confluent monolayers of BGM, Vero and Calu-3 cells in 6-well plates were incubated with viral stocks at a multiplicity of infection (MOI) of 0.01 for 2 h at 37°C followed by washing twice with PBS and maintained in RPMI 1640 medium with 2% FBS and HEPES (20 mM) at 37°C in a 5% CO₂ incubator. Culture supernatants were collected at the indicated time points and stored at –80°C for subsequent viral growth kinetics assay by quantifying the viral RNA copies and viral titres by using qPCR and 50% tissue culture infectious dose (TCID₅₀), respectively.

TCID₅₀ assay

BGM cells (2.5×10^4 cells/well) in 96-well plates were incubated together with ten-fold serial dilutions of the cell culture supernatants at 37°C in a 5% CO₂ incubator. Cytopathic effect was observed at 5 d.p.i.. Viral titres were calculated and were shown as TCID₅₀/mL.

RNA extraction and qRT-PCR analysis

Total viral RNA from cell culture supernatants was extracted by using the EasyPure® Viral DNA/RNA Kit (TransGen, Cat No. ER201-01 Beijing, China) according to the manufacturer's instructions. Reverse transcription was performed to produce complementary DNA (cDNA) using Hifair II 1st Strand cDNA Synthesis Kit (Yeasen Biotech, Cat No. 11123ES60, Shanghai, China), and then 2 µL cDNA was used as template for subsequent qPCR. The target N gene of GX_P2V (short_3UTR) was amplified by qPCR using FastFire qPCR PreMix (Probe) (TIANGEN, Cat No. FP208-02, Beijing, China) according to the manufacturer's instructions. Sequences of qRT-PCR primers are as follow: P2VF, TCTTCCTGCTGCAGATTTGGAT; P2VR, ATTCTGCACAAG-AGTAGACTATGTATCGT; and Probe, FAM-TGCAGACCACACAAGGCAGATGGGC-TAMRA. In addition, a standard plasmid was constructed through inserting a fragment amplified using P2VF and P2VR into a cloning vector pEASY-T1 (TransGen, Cat No. CT101-01 Beijing, China). Plasmids in a range of 10^2 – 10^8 DNA copies were used as template to generate a standard curve.

Immunofluorescence assay (IFA) for viral growth

Confluent monolayers of BGM and Calu-3 cells grown on coverslips in 12-well plates were incubated with GX_P2V at an MOI of 0.01 for two hours at 37°C in 5% CO₂, then washed twice with PBS and cultured in RPMI 1640 with 2% FBS and HEPES (20 mM) at 37°C in 5% CO₂. At indicated time points, the cells were washed twice with PBS and fixed with 4% paraformaldehyde for 20 min at room temperature, permeabilized by using 0.2% (vol/vol) Triton X-100 in PBS for 10 min, then blocked overnight with 3% bovine serum albumin (BSA) at 4°C. Then, cells were incubated with anti-sera (1:200, prepared in our laboratory) from GX_P2V(short_3-UTR)-infected hamsters for two hours at room temperature. After being washed five times with PBS, cells were stained with a fluorescein isothiocyanate (FITC)-labeled goat anti-mouse IgG antibody (1:300, ZSGB-BIO, Cat No. ZF-0312, Beijing, China) for one hour at room temperature. Cells were washed five times and stained with 4',6-Diamidino-2-phenylindole dihydrochloride (DAPI) (Sigma, Cat No. 10236276001, Germany) for 20 min. Finally, after being washed five times, cells on the coverslips were scanned and photographed using a fluorescence microscopy (Nikon, Japan).

Golden hamster model of both intranasal and intragastrical infection

Specific pathogen-free, 6-week-old male golden hamsters were purchased from Charles River and maintained

under specific-pathogen-free conditions. For intranasal infection, hamsters were infected with 1×10^4 or 1×10^5 TCID₅₀ of GX_P2V(short_3UTR) in 50 μ L RPMI 1640 containing 2% FBS after deep anesthesia with pentobarbital sodium. Equal volume of RPMI 1640 containing 2% FBS was set as mock-control group. The mock-infected group ($n = 3$) was monitored and sacrificed at 7 d.p.i.. In the GX_P2V(short_3UTR)-infected group ($n = 12$ per group), three hamsters were sacrificed at each indicated time points (2, 5, 7 and 14 d.p.i.). For intragastrical infection, hamsters were infected with 1×10^5 TCID₅₀ of GX_P2V(short_3UTR) in 100 μ L RPMI 1640 containing 2% FBS. Equal volume of PBS was used to mock-infect the control group. Mock-infected hamsters ($n = 4$) were sacrificed at 14 d.p.i., while four hamsters of GX_P2V(short_3UTR)-infected ($n = 20$) were sacrificed at each indicated time points (2, 5, 7, 9 and 14 d.p.i.).

After viral infection, various indexes were collected during a 14-day experimental period. The body weight changes and clinical symptoms were recorded before the hamsters were humanly euthanized [17]. Left lungs, bottom tracheas and other tissues (heart, liver, kidney, brain, duodenum, and small intestine) were placed in 4% paraformaldehyde and were stored at room temperature at least two days for observation of the pathological changes. The rest of the lungs and other tissues and sera samples were collected and frozen directly at -40°C for viral detection.

Intranasal infection in both young and aged BALB/c mice

Specific pathogen-free, 6-week-old male young BALB/c mice and 48-week-old female aged BALB/c mice were obtained from SiPeiFu (Beijing). Young and old mice were randomly divided into two groups, respectively. Mice were anesthetized intraperitoneally (i.p.) with pentobarbital sodium and then infected intranasally with 1×10^5 TCID₅₀ of GX_P2V(short_3UTR) in 30 μ L RPMI 1640 containing 2% FBS or PBS as control group. Mock-infected young ($n = 5$) or aged ($n = 3$) mice were sacrificed at 14 d.p.i., while five young or three aged GX_P2V(short_3UTR)-infected mice ($n = 25$ or 15, respectively) were sacrificed at each of the indicated time points (1, 3, 6, 9 and 14 d.p.i.). Body weight and clinical symptoms were assessed periodically. Blood samples and organ tissues were collected regularly. Some parts of tissues were fixed with 4% paraformaldehyde for determining histopathological changes. The rest of tissues were frozen directly at -40°C for analysing the viral loads and titres.

Measurement of viral RNA copies and virus titres in organ tissues

Lung, trachea, heart, liver, spleen, kidney, brain, stomach, duodenum, eyeball, tongue, turbinate,

small intestine, and feces specimens were homogenized in 10 μ L PBS per milligram of tissue for 60 s at 60 Hz 4 times using a TissueLyse-24 system (Jingxin, Shanghai). Tissue homogenates were centrifuged at $5,000 \times g$ at 4°C for 5 min. Total viral RNAs from tissue supernatants were extracted by using EasyPure® Viral DNA/RNA Kit (TransGen, Cat No. ER201-01, Beijing, China) for qRT-PCR analysis as noted above. Infectious titres in tissue supernatants were detected and calculated by TCID₅₀ assay as mentioned above. Virus titres were indicated as TCID₅₀/mL.

Histopathology of organ tissues

The lungs and tracheas were grossly examined and photographed before freezing and fixing. The other organ tissues were fixed in 4% paraformaldehyde and embedded in paraffin. The paraffin sections were prepared for H&E staining. The histopathology of the organ tissues was detected by microscopy (Nikon, Japan). The histopathological results were analysed by professional pathologists.

Anti-sera preparation from hamsters

Hamsters were intranasally challenged with two doses (1 and 21 d.p.i.) of 1×10^5 TCID₅₀ GX_P2V(short_3UTR). Sera were collected at 42 d.p.i. for analysis of antibody responses by immunofluorescence assay (IFA), ELISA, and pseudovirus neutralization titre assay (pVNT). Anti-sera were heated at 56°C for 30 min before use.

Immunofluorescence assay for cross-immunity responses

The full-length spike protein gene of SARS-CoV-2 (accession number NC_045512) and GX_P2V(short_3UTR) (accession number MW532698) were codon optimized, synthesized, and cloned into pcDNA3.1 vector by Beijing BioMed Gene Technology. Confluent monolayers of 293T cells grown on coverslips in 12-well plates overnight were transfected with plasmids containing codon-optimized spike genes of SARS-CoV-2 and GX_P2V(short_3UTR) by using liposome (TransGen, Cat No. FT201-02, Beijing, China) according to the instructions. After five hours, the cells were washed twice with PBS and cultured in DMEM with 2% FBS at 37°C in 5% CO₂. After 36 h post-transfection, cells were fixed, permeabilized, and blocked. Then, cells were incubated with sera from GX_P2V(short_3UTR)-infected hamsters (1:200), convalescent COVID-19 patients (1:200), mock-infected hamsters, or healthy donors. After being washed five times with PBS, cells were stained with secondary antibodies: fluorescein isothiocyanate (FITC)-labeled

goat anti-mouse IgG (1:300, ZSGB-BIO, Cat No. ZF-0312, Beijing, China) or goat anti-human IgG (1:300, ZSGB-BIO, Cat No. ZF-0308, Beijing, China), accordingly. Following five washes with PBS, cells were stained with DAPI (Sigma, Cat No. 10236276001, Germany) for 10 min. Finally, after being washed five times, cells on the coverslips were analysed using fluorescence microscopy (Nikon, Japan).

ELISA binding assay

SARS-CoV-2 RBD, S1 and S1 + S2 (ECD) antibody titre assay kits (Sino Biological, Cat No. KIT002, KIT003, KIT004, respectively, Beijing, China) were purchased. Experiments were carried out following the manufacturer's instructions with minor modifications. All sera were diluted with dilution buffer at a ratio of 1:100. Patient's sera were tested according to the instructions. For testing sera from hamsters and BALB/c mice, the secondary antibodies were replaced by HRP-goat anti-mouse IgG (1:5,000, ZSGB-BIO). Plates were read at 450 nm wavelength on a synergy H4 hybrid reader (Biotek, USA).

Pseudotyped virus neutralization assay

The VSV-based SARS-CoV-2 pseudovirus was kindly provided by Prof. Youchun Wang (National Institutes for Food and Drug Control). The SARS-CoV-2 pseudovirus was used as seed stock and combined with the GX_P2V(short_3UTR) spike protein expression plasmid to generate VSV-based GX_P2V pseudovirus in 293T-hACE2 cells. The pseudovirus based neutralization assay procedure was conducted as previously described with minor modifications [18]. Briefly, sera samples were diluted in five three-fold serial dilutions and incubated with 1 000 TCID₅₀ of pseudovirus in 96-well plates, making the initial dilution 1:30. After one hour of incubation at 37°C, cells (2.5×10^4 cells/well) were added and incubated for another 24 h at 37°C in a CO₂ incubator. Cells were lysed by adding luciferase substrate (PerkinElmer, USA). Luciferase activity was then measured using a synergy H4 hybrid reader (Biotek, USA). The 50% neutralization titre (NT₅₀) was calculated for each individual serum sample by using the Reed-Muench method.

Statistical analysis

The statistical analyses were performed with Graph-Pad Prism version 9.0 software. The differences of two groups were analysed by two-tailed Student *t*-test. The *p*-values of less than 0.05 ($p < 0.05$) were considered statistically significant.

Results

Genomic determination of pangolin coronavirus GX_P2V isolate

Total RNAs from the eighth viral passage were used for Illumina pair-end sequencing. In total, 8,482,736 reads were mapped to the previous genome of GX_P2V using Bowtie 2. The resulting viral reads were then assembled *de novo* by Trinity. The viral genomic contig has 29,718 nucleotides including eight consecutive adenine residues at the 3'-terminus. The 5'-terminus of the viral genome was determined by 5'/3' RACE kits (TaKaRa) and the whole genome sequence (29,729 nt) was deposited in GenBank (accession number MW532698).

Genomic comparison between the GX_P2V sample and the coronavirus GX_P2V isolate revealed two mutations in the passaged viral isolate

We next compared the sequence differences between the first passage of the GX_P2V sample and the eighth passage of the GX_P2V isolate. Compared to the single cell-passaged sample, the multiply passaged GX_P2V isolate has complete 5'/3'-terminus sequences and two mutations: a nonsynonymous mutation in the final amino acid codon of the nucleoprotein gene (GCU→GUU) and a 104-nucleotide deletion in the hypervariable region (HVR) of the 3'-terminus untranslated region (3'-UTR) (Figure 1). Thus, the multiply passaged GX_P2V isolate is a cell culture adapted variant. The result of the single-nucleotide mutation is an alanine to valine change at the carboxyl terminal of the nucleoprotein. We then asked whether these two mutations occurred in the first passage of the GX_P2V in Vero cells. Among the sequencing reads of the GX_P2V sample (SRR11093271), only one read contained the nucleoprotein single-nucleotide mutation while no reads contained the HVR deletion. In comparison, among the sequencing reads of the multiply passaged isolate (renamed GX_P2V(short_3UTR)), all reads covering these two mutated regions contain the identified mutations. These data suggest that these two identified regions have strong selection pressures in cell culture and selection occurred rapidly following *in vitro* growth.

The temporal occurrence and selective factor(s) for these mutations are unknown. It is plausible that both mutations increased the efficiency of viral replication. The spontaneous 104-nt deletion within the viral 3'-UTR is of special interest. According to the current 3'-UTR model [19], the HVR region of the GX_P2V sample is 166-nt long – ranging from 29,611–29,776 based on the deposited sequence data (GenBank

A

SARS-CoV-2: UUG CAA CAA UCC AUG AGC AGU GCU GAC UCA ACU CAG GCC UAA
 GX_P2V sample:UU ...
 GX_P2V isolate:UUU ...

B

SARS-CoV-2: UUAUUCUCACAUAGCAAUCUUUAUUCAGUGUGUAACAUAUAGGGAGGACUUGAAAG
 GX_P2V sample:
 GX_P2V isolate:-----

SARS-CoV-2: AGCCACCACAUUUUCACCGAGGCCACGCGGAGUACGAUCGAGUGUACAGUGAACA
 GX_P2V sample:G.....U.
 GX_P2V isolate: -----

SARS-CoV-2: AUGCUAGGGAGAGCUGCCUAUAUGGAAGAG
 GX_P2V sample:
 GX_P2V isolate: -----

Figure 1. Sequence comparisons between SARS-CoV-2, the original GX_P2V sample and the pangolin coronavirus GX_P2V isolate. The GX_P2V isolate (GX_P2V(short_3UTR)) is a variant with two interesting mutations: one nonsynonymous mutation (C to U) in the final amino acid codon of the nucleoprotein and one 104-nt deletion in the 3'-UTR. (A) Alignment of the 3'-terminus sequences of the nucleoprotein genes. (B) Alignment of the partial 3'-UTR sequences. Dots represent residues that are identical to those in SARS-CoV-2 and hyphens represent nucleotide deletions.

accession number MT072864). The deletion region ranges from 29,617–29,720, covering 62.7% of the entire HVR region. The HVR region is absolutely maintained in all coronavirus clinical samples. Based on our knowledge, this is the first report of a spontaneous deletion in the HVR region.

Growth of the pangolin coronavirus GX_P2V variant yields mild cell damage and small plaques in non-human primate cells, and no cytopathic effects or plaques in human Calu-3 cells

The GX_P2V isolate was cultured from a mixture of pangolin lung and small intestine samples by using Vero E6 cells [6]. It has been shown that the virus only partially destroys Vero E6 cell monolayer five days post-infection [6]. In cells infected with the virus for five days, the cytopathic effects manifested as cell degeneration and cell lysis, with significant portion of cell rounding but limited cell detachment. We next systematically investigated the growth of GX_P2V(short_3UTR) in two non-human primate cells (Vero and BGM) and human Calu-3 cells. The BGM and Calu-3 cells were selected based on the fact that they are highly susceptible to SARS-CoV and the pangolin viruses GX/2017 utilize ACE2 as the cell receptor for viral attachment and entry [11, 20].

BGM, Vero and Calu-3 cells were infected with GX_P2V(short_3UTR) at a multiplicity of infection (MOI) of 0.01. Growth of GX_P2V(short_3UTR)

induced similar cytopathic effects in both Vero and BGM cells (Figure 2(A)). No or limited cell degeneration can be observed at 24 h postinfection. More evident cell degeneration and cell rounding appeared at 48 h postinfection. Cell lysis and detachment started around 72 h postinfection. These cytopathic effects were directly related to viral replications, which was confirmed by indirect immunofluorescence (Figure 2 (B)). Consistent with the observed slow rate of cell damages, GX_P2V(short_3UTR) produced small plaques on Vero and BGM cells at five days postinfection (Figures 2(C–D)). In comparison, SARS-CoV-2 produced substantial cell damages and large plaques in Vero cells at two days postinfection [4, 21]. Notably, GX_P2V(short_3UTR) showed no visible cytopathic effects or plaques in Calu-3 cells (Figure 2(A–C)). Compared to reported SARS-CoV-2 data, GX_P2V (short_3UTR) is highly attenuated in causing cell damage and plaque formation.

The growth kinetics of GX_P2V(short_3UTR) in BGM, Vero and Calu-3 cells were measured by quantifying the viral RNA copies and viral titres in the culture supernatants by using qPCR and viral titration, respectively (Figure 3). Cells were infected with a MOI of 0.01. Supernatants were collected at indicated time points and were used for quantification assays. In all cells, the viral RNA copies reached the peak at 72 h.p.i. (Figure 3(A)) and the peaks of viral titres were at 48 h.p.i. (Figure 3(B)), though only limited or no cell degenerations could be observed at this time point. The viral titres at 48 h.p.i. were as high as 10^7 TCID₅₀/mL –a titre number that is comparable to

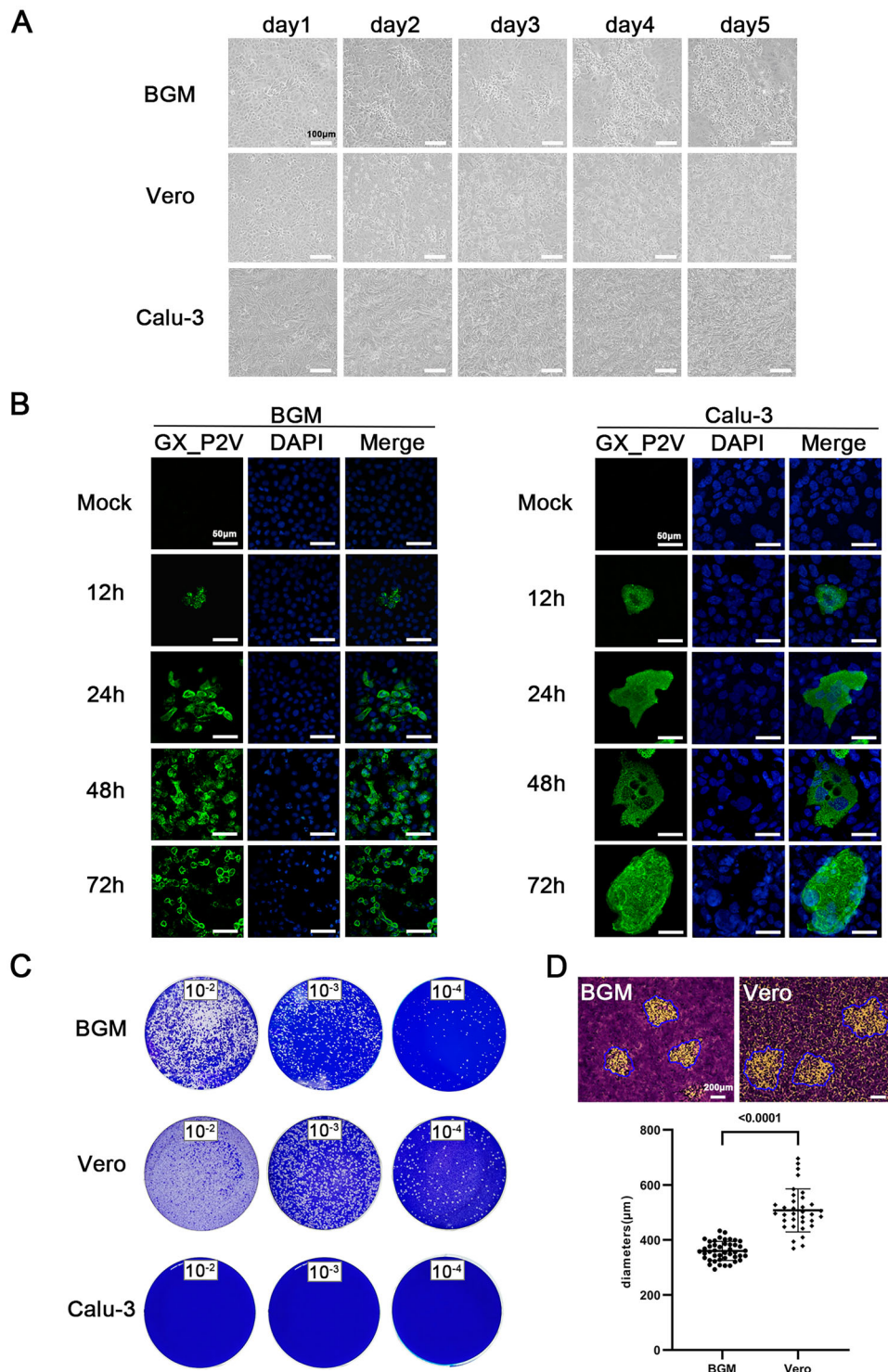


Figure 2. Growth of the pangolin coronavirus GX_P2V variant in two non-human primate cells (BGM and Vero) and human Calu-3 cells. (A) BGM and Vero cells infected with GX_P2V(short_3UTR) show similar cytopathic effects: limited cell degeneration at 24 h postinfection, and more evident cell degeneration and cell rounding after 48 h postinfection. Calu-3 cells infected with GX_P2V(short_3UTR) showed no cytopathic effects. Scale bars, 100 µm. (B) The replication of GX_P2V(short_3UTR) in BGM and Calu-3 cells at different time points was detected by immunofluorescence assays with anti-sera from GX_P2V(short_3UTR)-infected hamsters. Nuclei were stained with DAPI (blue). Scale bars, 50 µm. (C) GX_P2V(short_3UTR) forms small plaques in BGM and Vero cells at five days postinfection, while no plaque was produced in Calu-3 cells. The small white dots represent plaques. (D) The diameter of plaques (blue circle) was measured by using Image Pro plus 6.0 software. GX_P2V(short_3UTR) forms bigger plaques in Vero than in BGM ($p < 0.0001$).

the titre of SARS-CoV-2 at this time point [21]. The growth curves of GX_P2V(short_3UTR) in three cells are similar, but do have significant differences at 24 and 120 h.p.i. (Figure 3(B)). Higher viral titres

were detected in Vero cells at 120 h.p.i. ($p < 0.001$). Consistent with this difference, Vero cells were more supportive of viral plaque assays, as they have more cell lysis starting at 72 h.p.i. and produced larger

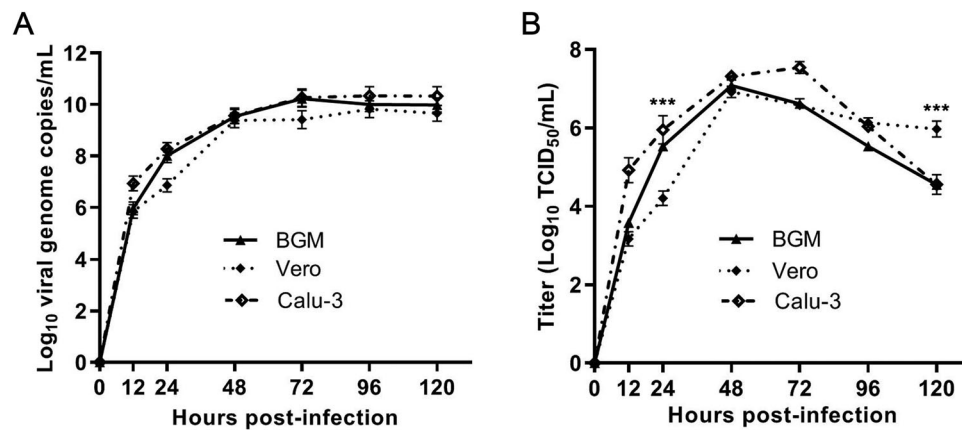


Figure 3. Replication kinetics of GX_P2V(short_3UTR) in BGM, Vero and Calu-3 cells. Results are expressed as the mean of three biological replicates. (A) Viral RNA copies were determined by qRT-PCR. (B) Viral titres were titrated by using a standard TCID₅₀ assay. Compared to BGM and Calu-3, Vero cells appear to produce different viral titres at 24 and 120 h postinfection (***p* < 0.001).

viral plaques at 120 h.p.i. (0.36 ± 0.04 mm v.s. 0.51 ± 0.08 mm, *p* < 0.0001) (Figure 2(A and D)).

The pangolin coronavirus GX_P2V variant is highly attenuated in the golden hamster intranasal infection model

Studies on SARS-CoV-2 pathogenesis provide animal models for investigating the pathogenicity of GX_P2V (short_3UTR) [22–24], as its spike protein has similar capabilities of binding to human ACE2 [11]. The golden hamster model is especially susceptible to SARS-CoV-2. SARS-CoV-2 administered by intranasal route can replicate efficiently in the lungs of hamsters, causing severe pathological lung lesions [23]. These severe lung injuries shared characteristics with SARS-CoV-2-infected human lungs, including severe, bilateral, peripherally distributed, multilobular ground glass opacity, and regions of lung consolidation [23, 24]. We next investigated the replicative ability and pathogenesis of GX_P2V(short_3UTR) in golden hamsters.

Three groups of hamsters were intranasally infected with mock, 1×10^4 and 1×10^5 TCID₅₀ of GX_P2V (short_3UTR), respectively. Clinical signs were recorded and samples were collected periodically throughout the 14-day experiment (Figure 4(A)). The infection outcomes are clearly contrast to those described in the SARS-CoV-2 infected hamsters. Hamsters infected with GX_P2V(short_3UTR) had similar body weight increases to the mock infected hamsters and no apparent clinical symptoms in the two week observational period (Figure 4(B)). Consistent with the absence of clinical manifestations, there was only a slight hyperemia noted on the surface of lungs following infection with GX_P2V(short_3UTR) at 2 and 5 d.p.i. (Figure 4(C)). Moreover, no signs of bronchopneumonia were found in the tracheas of infected hamsters (Figure 4(C)).

To monitor the viral replication and pathogenesis, heart, liver, stomach, kidney, eyeball, brain, duodenum, small intestine, tongue, feces, blood, turbinate, lung and trachea tissues of hamsters were collected at indicated time points. Viral RNA copies and viral titres were measured. In turbinate, lung and trachea tissues, viral RNA copies peaked at two d.p.i. and gradually decreased for the remaining days (Figure 4(D–F)). The RNA copy numbers at two d.p.i. were larger than the original inoculum numbers, demonstrating replication in turbinates, lungs and tracheas. However, viral titres were only detected in early stages post-infection: at two and five d.p.i. in lungs and turbinates, and day two in tracheas (Figure 4(G–I)). Limited viral RNAs, not viral titres, were detected in other extrapulmonary tissues and feces (Figure S1). This suggests a shorter duration of viral replication in pulmonary, not extrapulmonary, tissues.

Hematoxylin and eosin staining was performed to determine the histopathological changes in heart, liver, kidney, brain, duodenum, small intestine, turbinate, lung and trachea tissues. Histopathologically, lungs from hamsters of the 1×10^4 TCID₅₀ group were comparable to sham infected controls (Figure 5(A)). Infection with 1×10^5 TCID₅₀ of GX_P2V (short_3UTR) resulted in a local infiltration with very few inflammatory cells in lungs at five d.p.i., and none at other time points (Figure 5(B)). Compared to the mock group, no pathological lesions were found in all the tissues of all GX_P2V(short_3UTR)-infected hamsters over the entire observation period (Figure 5(C and S2)). Thus, GX_P2V(short_3UTR) did not induce potentially damaging inflammatory changes in any tissues of either infected groups. The lack of detectable pathology and short duration of viral replication in infected hamsters suggests that GX_P2V(short_3UTR) has a replicative deficiency in hamsters.

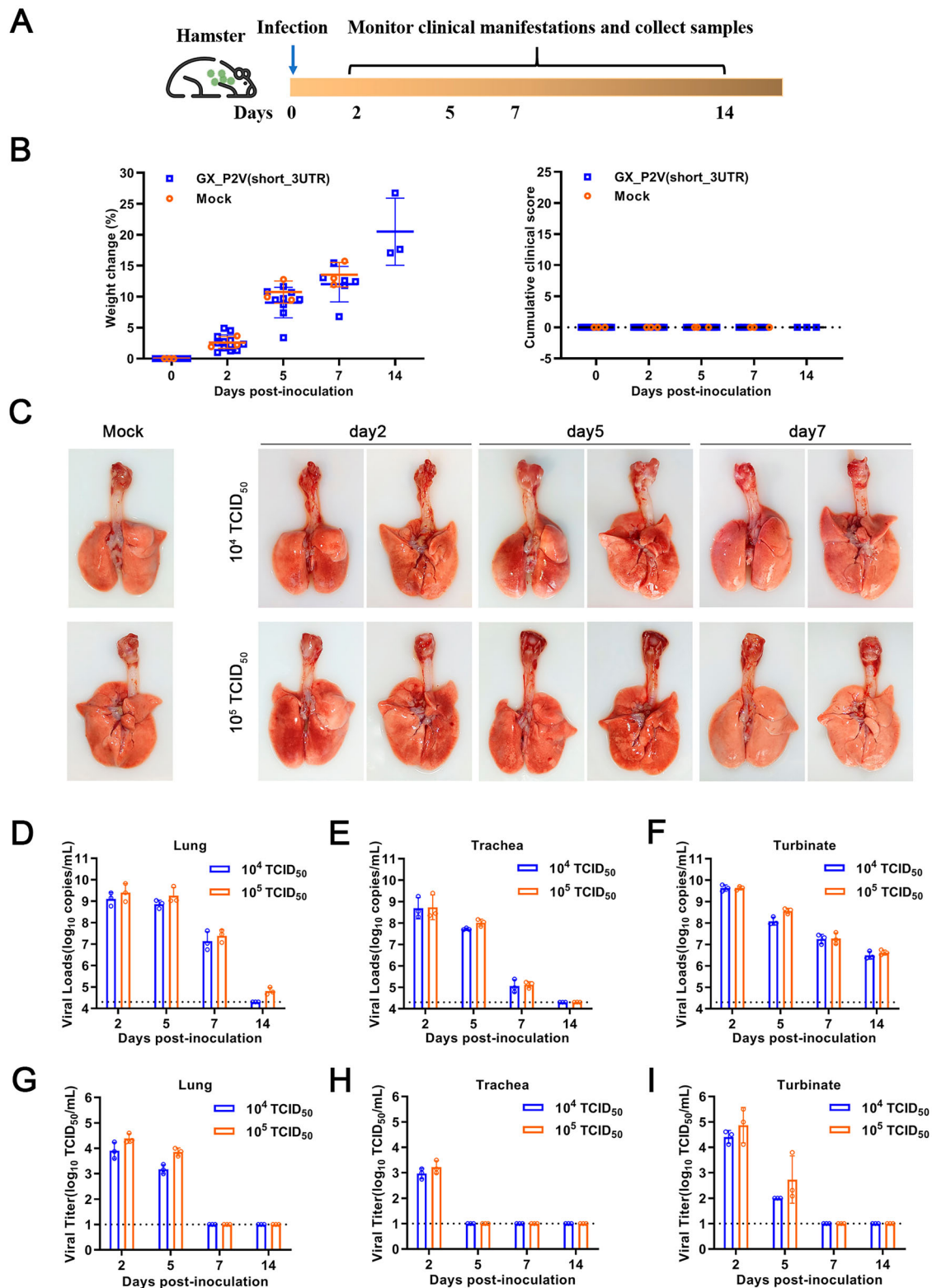


Figure 4. Intranasal infection of golden hamsters shows GX_P2V(short_3UTR) had a short duration of viral replication and caused no gross pathology in the respiratory tracts. (A) Scheme of intranasal infection. (B) Both mock and GX_P2V (short_3UTR)-infected hamsters had normal body weight increases and no apparent clinical symptoms in the two-week observational period. Individual data points represent percent weight changes from mock hamsters, 1×10^4 , and 1×10^5 TCID₅₀ infected hamsters at indicated time points. All organs had no gross pathology. (D-I) Viral RNA loads (D-F) and viral titres (G-I) in homogenate supernatants of lungs (D, G), tracheas (E, H) and turbinates (F, I) of GX_P2V(short_3UTR)-infected hamsters at different days post-inoculation were determined by qRT-PCR and the TCID₅₀ assay, respectively. The detection limit is shown by the dotted line. Error bars represent means \pm SD.

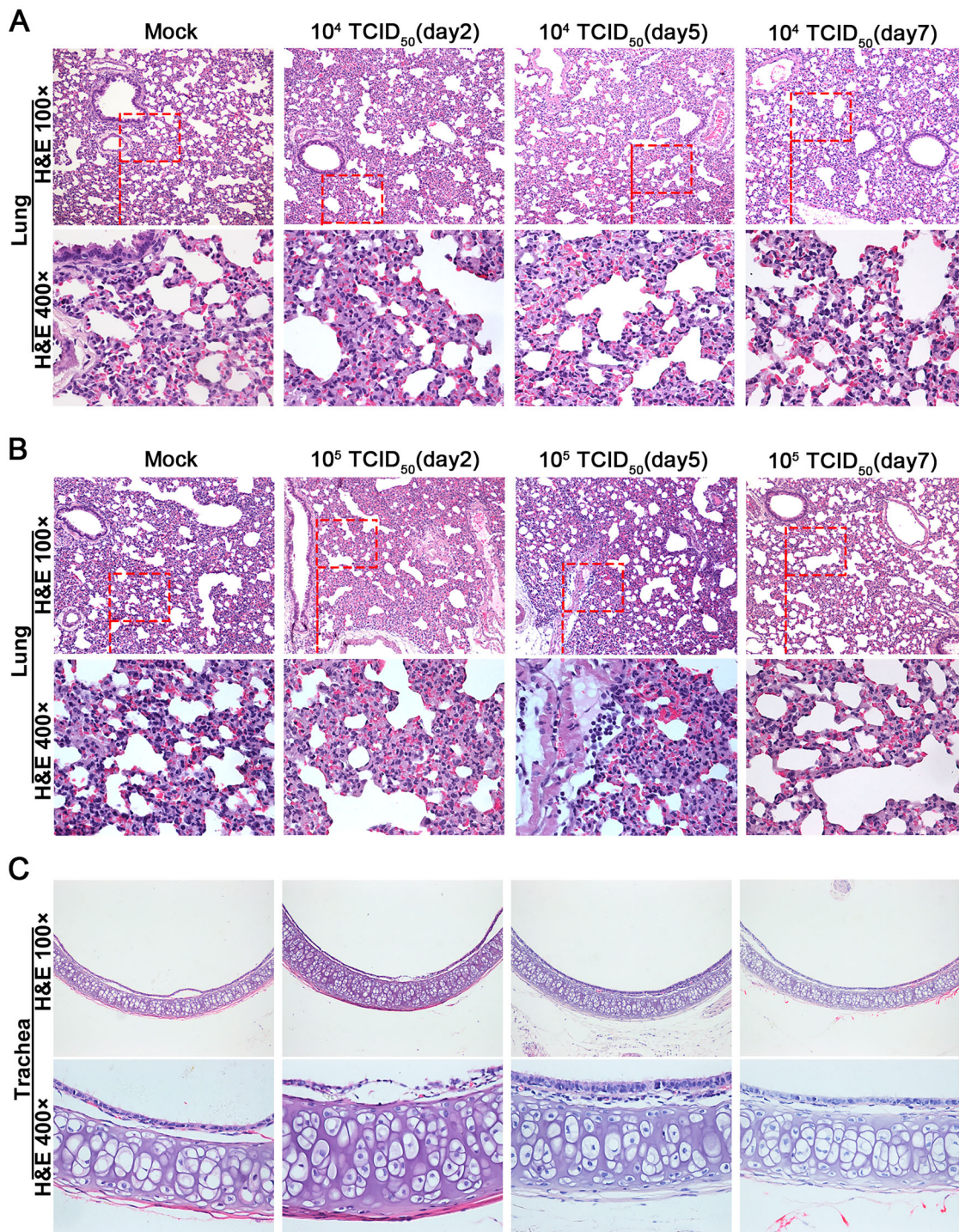


Figure 5. Histopathological analyses of lung and trachea tissues from intranasally infected hamsters. H&E 400 × are the magnifications of the region in the corresponding red box in H&E 100 × . (A) 1×10^4 TCID₅₀ infected group (n = 3), no pathological changes were observed in the lungs. (B) 1×10^5 TCID₅₀ infected group (n = 3), lungs had no tissue lesions. Few inflammatory cells of lymphocytes and neutrophils associated with blood vessels were observed at five days postinfection but not at other time points. (C) Representative images show that tracheas of both infection dose groups had no significant histopathological changes at all time points post-infection.

Intragastrical inoculation established limited infections in respiratory tracts but no detectable infection in the gastrointestinal tract

Human gastrointestinal (GI) infection by SARS-CoV-2 has been implied, as SARS-CoV-2 RNA can be frequently detected in the feces of COVID-19 patients [25]. In the golden hamster model, oral

inoculation can establish a SARS-CoV-2 infection with an infection pattern that is consistent with mild COVID-19 [26]. In the above described intranasal infection of golden hamsters with GX_P2V (short_3UTR), viral RNA sheddings were detected in tongues and feces only at the earliest times post inoculation (Figure 6(A)), which is different than

the continuous RNA sheddings in COVID-19 patients. We performed intragastrical inoculation of GX_P2V(short_3UTR) in golden hamsters to further assess viral pathogenicity. Golden hamsters were intragastrically infected with 10^5 TCID₅₀ of GX_P2V(short_3UTR) and samples were collected periodically (Figure 6(B)). All hamsters had consecutive weight increases (Figure 6(C)) and no apparent clinical signs were observed (Figure 6(D)). Limited viral RNAs were detected in lungs but not in other organs or samples (stomachs, duodenums, colons, tongues, trachea, esophaguses, small intestines and feces) (Figure 6(E)). Thus, the virus shedding of GX_P2V(short_3UTR) in golden hamsters differs from the chronic virus shedding from the oral cavity and feces following oral inoculation of SARS-CoV-2 [26]. Predictably, no histopathological changes were detected in lungs of intragastrically infected hamsters (Figure 6(F)). Similar to previous reports with SARS-CoV-2 in golden hamsters [26], we failed to detect infectious virus in fecal samples from either intranasal or intragastrical infections (Figure 6(G)). Thus, in golden hamsters, GX_P2V(short_3UTR) has limited capability of establishing infections of the gastrointestinal tract or when introduced by the intranasal route.

The GX_P2V variant does replicate but produce no infectious virus in young and aged BALB/c mice

SARS-CoV-2 can rapidly adapt in aged BALB/c mice and induce typical pneumonia [27, 28]. Therefore, we next investigated the pathogenicity of GX_P2V (short_3UTR) in both young and aged BALB/c mice. BALB/c mice were intranasally infected with 1×10^5 TCID₅₀ of GX_P2V(short_3UTR) and euthanized to collect samples at specific days postinfection (Figure 7(A)). Following inoculation, no apparent clinical signs were observed in any inoculated mice. Notably, the body weights of young BALB/c mice continued to increase (Figure 7(B)) and no gross pathological changes on the lung surfaces of inoculated mice were detected (Figure 7(C)). The viral RNAs in the lung, turbinate, and trachea tissues of young mice were rapidly cleared, and aged mice had an even faster rate of viral clearance (Figures 7(D and S3)). This is in contrast to the slower rate of viral clearance in aged mice inoculated with SARS-CoV-2 [27]. Histopathological analyses suggest that lymphocytes play an important role in the rapid viral clearing (Figures 7(E-F)). Lungs of the inoculated young mice had local thickened alveolar septa

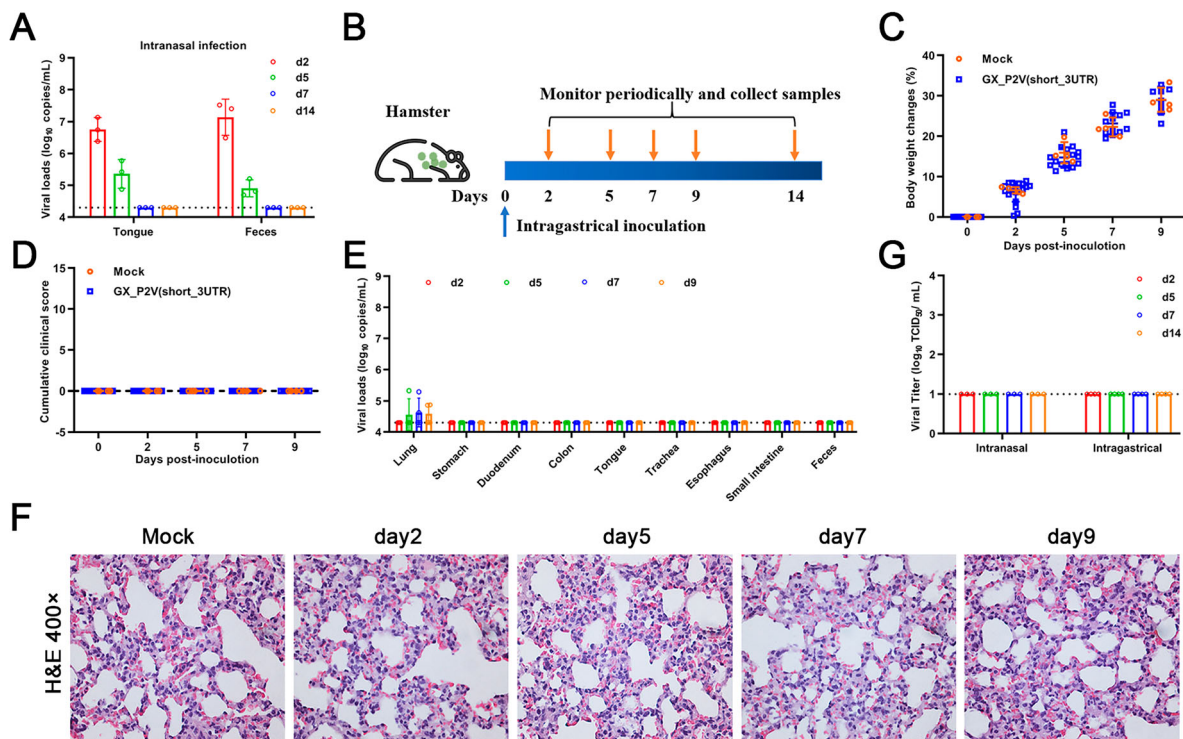


Figure 6. Intra-gastrical inoculation of GX_P2V(short_3UTR) in golden hamsters established limited infection in the respiratory tract. (A) Viral RNAs were detected in samples of tongues and feces from the above golden hamsters with intranasal infection, suggesting established infections in the gastrointestinal tract. (B) Scheme of intragastrical infection. Samples of tongues and feces were collected at indicated time points. (C) Body weights of all golden hamsters had continuous increases. (D) No clinical symptoms of infection were identified. (E) Limited viral RNAs in the lungs, but not in other organ tissues were detected by qPCR. (F) No histopathological changes were identified in lung tissues of mock and GX_P2V(short_3UTR)-inoculated golden hamsters. (G) Viruses were not detected in feces from golden hamsters following intranasal or intragastrical inoculation.

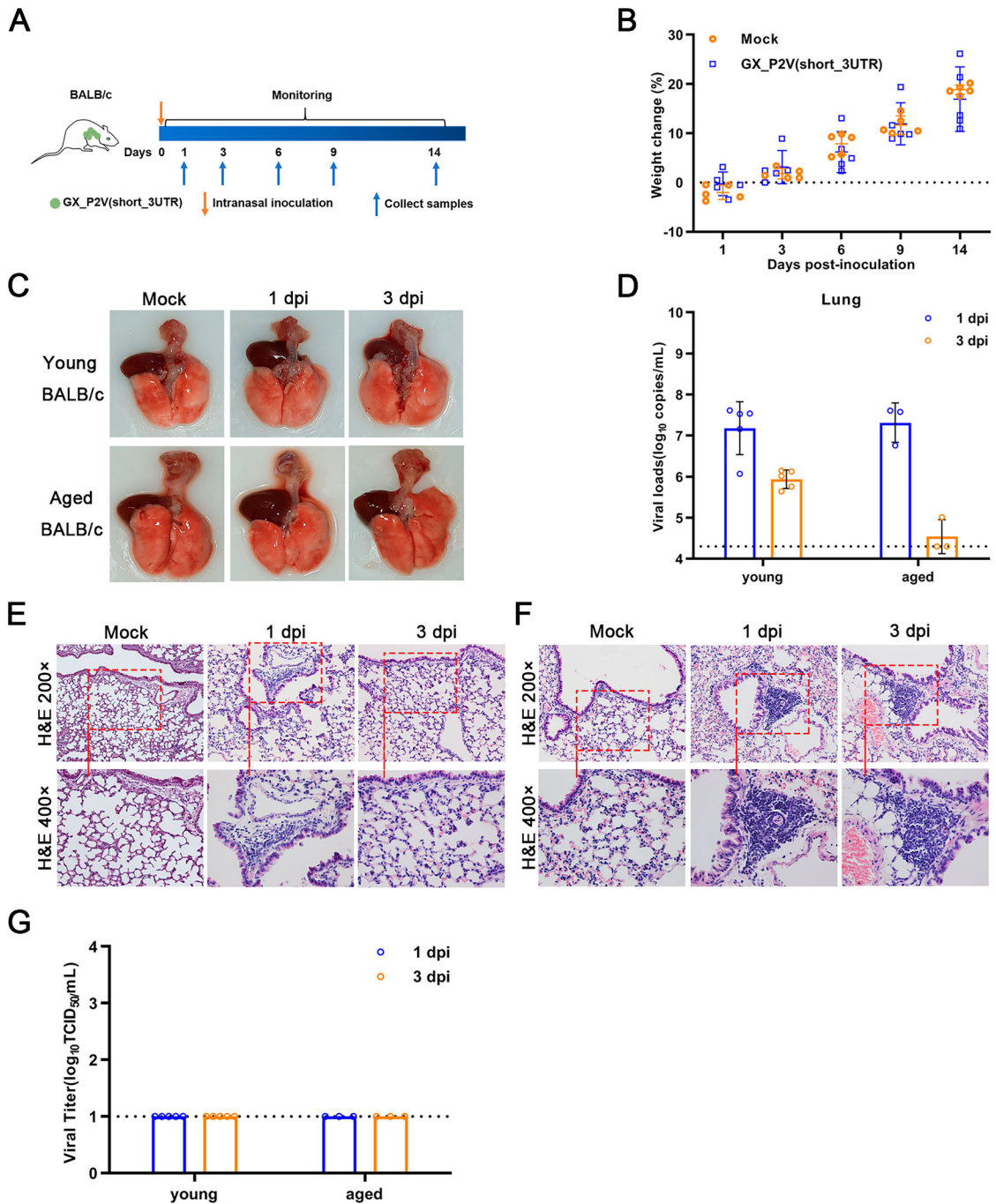


Figure 7. Intranasal inoculation of GX_P2V(short_3UTR) in both young and aged BALB/c mice. (A) Scheme of intranasal infection. Young and aged BALB/c mice were intranasally infected with mock or 1×10^5 TCID₅₀ of GX_P2V(short_3UTR). Various infection outcomes and tissue samples were collected at indicated time points. (B) Young mice had constant body weight increases after infection. (C) Intranasal inoculation of GX_P2V(short_3UTR) in young and aged BALB/c mice produce no detectable gross pathology. (D) Viral RNA loads in infected lungs of both young and aged BALB/c mice were determined by qPCR. (E-F) Representative H&E images of infected lungs from young (E) and aged (F) BALB/c mice. (G) No viral titres were detected in infected lungs from both young and aged BALB/c mice.

and lymphocyte aggregations at one d.p.i., then rapidly returned to normal at three d.p.i. (Figure 7 (E)). Comparatively, the lungs of the inoculated aged mice showed multifocal abundant lymphocytes and some macrophages present up to day three d.p.i. (Figure 7(F)). Furthermore, we failed to detect any infectious virus in lungs, despite detection of high viral RNA copies at the early infection time

points (Figure 7(G)). Similarly, high or low levels of viral RNAs, not viral titres, were detected in turbinate, trachea and other tissues (Figure S3). The histological characteristics in tissues from young BALB/c mice infected with GX_P2V(short_3UTR) are as normal as the control group (Figure S4). Altogether, our data indicate that GX_P2V(short_3UTR) can infect but has a replication deficiency in BALB/c mice.

Productive infections in golden hamsters induced neutralizing antibodies against both GX_P2V SARS-CoV-2

The coronavirus GX_P2V has high genomic homology with SARS-CoV-2 [6]. The spike protein and the receptor binding domain of GX_P2V share 92.4% and 86.8% amino acid identity with those of SARS-CoV-2, respectively. The attenuating nature of GX_P2V(short_3UTR), combined with its similarity to SARS-CoV-2, led us to propose that GX_P2V(short_3UTR) is a potential live vaccine candidate. To address, we analysed the humoral responses against GX_P2V in infected animals and evaluated cross-reactive antigenicity of the two spike proteins from GX_P2V and SARS-CoV-2.

Cells transfected with the full-length genes of the two spike proteins were used to perform immunofluorescence assays with sera from both convalescent COVID-19 patients and intranasally infected golden hamsters (Figure 8(A)). The results clearly show that these two spike proteins share strong cross-reactive antigenicity. Commercial SARS-CoV-2 S1 antibody assay kits can be used to titrate the humoral responses against GX_P2V in hamsters (Figure 8(B)). The intranasally infected hamsters have a strong humoral response to the spike protein. Such strong immune responses correlate with the productive infections in intranasally infected hamsters. In contrast, low titre or no antibodies against the spike protein were detected in intragastrically infected hamsters or intranasally infected BALB/c mice (Figure 8(C)).

SARS-CoV-2 neutralizing antibodies play an important role for the protection against COVID-19. We analysed the neutralizing antibodies in sera from COVID-19 convalescent patients, vaccinees of inactivated COVID-19, and intranasally infected hamsters by using pseudoviruses of GX_P2V and SARS-CoV-2 (Figure 8(D)). All tested positive sera had variable titres of neutralizing antibodies against both pseudoviruses. When compared to sera from convalescent patients, the hamster sera had a similar titre of neutralizing antibodies against SARS-CoV-2, although the RBDs of GX_P2V and SARS-CoV-2 share only 86.8% amino acid identity and share a single critical receptor-binding residue [6]. This finding supports the rationale for the design of pan-SARS-CoV-2 vaccines.

Discussion

The devastating force of COVID-19 intensified the world's fear over SARS-CoV-2 and its related coronaviruses. The search and characterization of SARS-CoV-2 related coronaviruses is an area of intense interest. In this study, we investigated the genome,

biology, pathogenicity, and cross-reactive antibody response of a SARS-CoV-2 related pangolin coronavirus GX_P2V(short_3UTR). We found that GX_P2V(short_3UTR) is a 3'-UTR shortened mutant derived from the original GX_P2V sample. GX_P2V(short_3UTR) was highly attenuated in three cell cultures, golden hamsters, and BALB/c mice. Importantly, the antibody elicited by GX_P2V(short_3UTR) infection in hamsters inhibited SARS-CoV-2 spike-pseudovirus infection. Attenuation and cross-neutralizing activity of the GX_P2V(short_3UTR) provides new insights for our understanding of coronavirus pathogenesis and for developing a live attenuated vaccine for SARS-CoV-2. Unfortunately, the original wild type GX_P2V virus was not isolated thus it could not be comparably studied. Nevertheless, this study represents the first report of characterizing SARS-CoV-2 related coronavirus in animal models.

In cell cultures, attenuation of GX_P2V(short_3UTR) caused mild cell damage and small plaques in two non-human primate cells, and no cytopathic effects or plaques in human Calu-3 cells. The attenuation is likely independent of viral infectivity, as the spike proteins of GX_P2V and SARS-CoV-2 have comparable capabilities of mediating cell attachment and entry [11]. It is also likely viral replication and egress were unaffected, as titres of live GX_P2V in the supernatants reach similar levels at 48 h.p.i. as SARS-CoV-2 [21, 29]. How could GX_P2V produce these attenuating phenotypes while having growth capabilities similar to those of SARS-CoV-2? Certain mutations in the spike protein have been linked with viral plaque sizes in SARS-CoV-2 [29]. Therefore, it is possible the spike protein of GX_P2V is less effective in host cell interactions than that of SARS-CoV-2.

The attenuation of GX_P2V(short_3UTR) in animal models can be explained by two aspects of our findings. The first is the 104-nucleotide deletion in the HVR of the 3'-UTR of the GX_P2V(short_3UTR). In the mouse hepatitis virus (MHV) model, the association between HVR mutations and viral pathogenicity has been comprehensively investigated [30]. MHV with a deletion of the entire HVR had minimal change on viral growth in cell cultures, but was highly attenuated in mice, causing no signs of clinical disease [30]. The HVR of GX_P2V likely also plays a significant role in viral pathogenesis. Its interactions with host cell factors warrants further investigations. Another aspect is the lower inner shell disorder in GX_P2V as predicted by measuring the percentage of protein intrinsic disorder of the nucleoprotein [31]. Goh et al predicted that the wild type GX_P2V virus was an attenuated SARS-CoV-2 vaccine strain even though the virus was initially identified in dead pangolins [31].

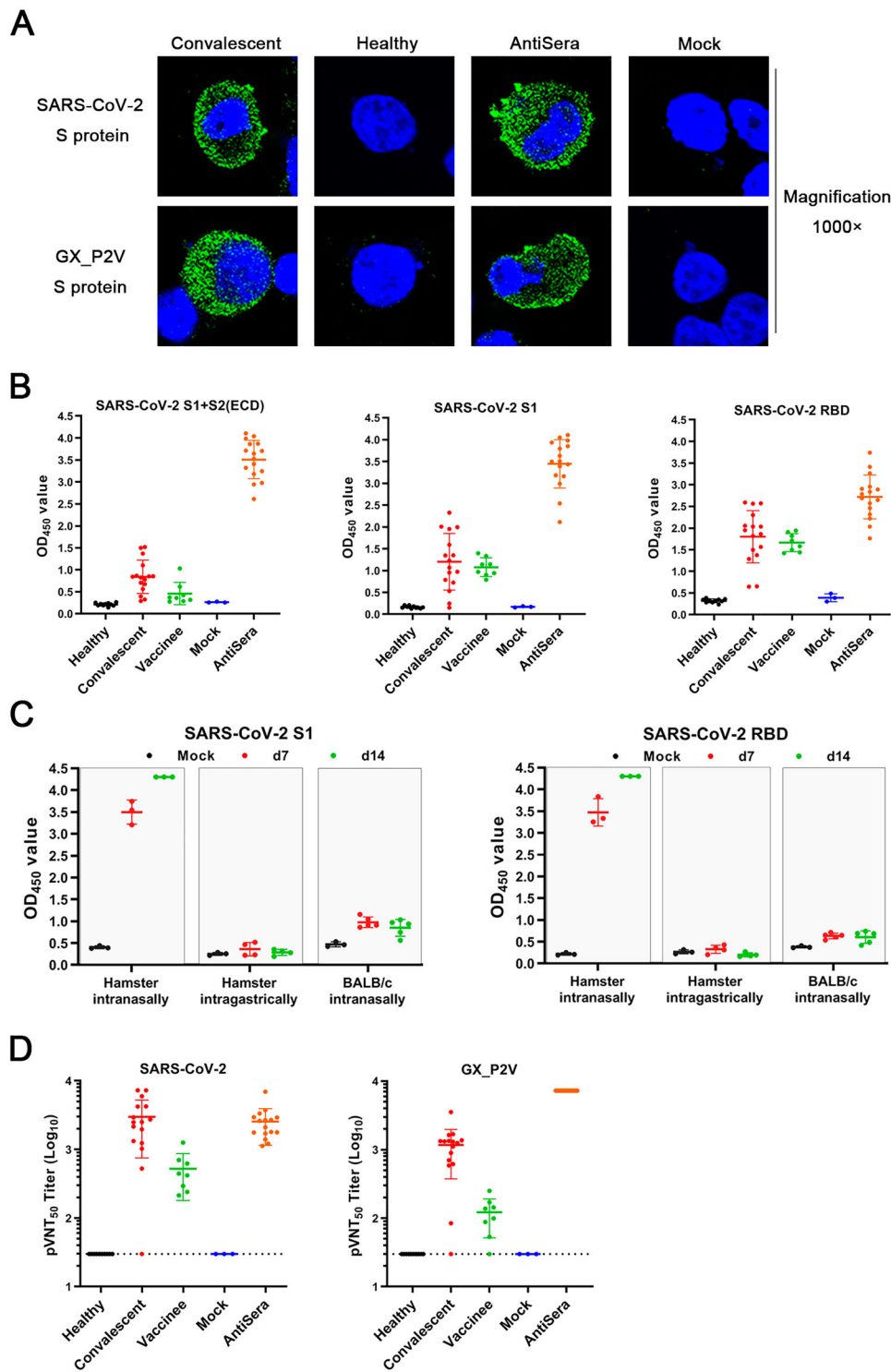


Figure 8. Serological cross-reactivity and cross-neutralization between GX_P2V and SARS-CoV-2. (A) Immunofluorescence assays with 293T cell expressing spike proteins (green) of SARS-CoV-2 and GX_P2V, using sera from convalescent COVID patients, healthy donors, and GX_P2V(short_3UTR)-infected golden hamsters. Nuclei were stained with DAPI (blue). (B) Three commercial ELISA kits for detecting antibodies against SARS-CoV-2 S1 + S2 (ECD), S1, and RBD were used for measuring antibodies in sera from healthy donors ($n = 10$), convalescent COVID patients ($n = 16$), vaccinees of inactivated COVID-19 vaccines ($n = 8$), mock-infected golden hamsters ($n = 3$), and GX_P2V(short_3UTR)-infected golden hamsters ($n = 16$), respectively. (C) Cross-reacting antibodies against SARS-CoV-2 S1 and RBD in sera from GX_P2V(short_3UTR)-infected golden hamsters and BALB/c mice were measured by using the aforementioned ELISA kits. No cross-reacting antibodies against SARS-CoV-2 S1 and RBD were detected in sera from intragastrically infected golden hamsters or intranasally infected BALB/c mice. (D) Neutralizing antibodies against two pseudo-viruses, SARS-CoV-2 and GX_P2V, were detected in sera as described in Figure 8(B). The error bars indicate means \pm SD.

The golden hamsters can be infected by both SARS-CoV and SARS-CoV-2, but disease outcomes varied by different strains and different infection routes [5,

9, 32]. Hamsters intranasally inoculated with a SARS-CoV Urbani strain had robust viral replication, with significant pathology in the respiratory tract, but

without weight loss or evidence of disease [32]. A follow-up study reported a lethal SARS-CoV Frk-1 strain, which differs from the Urbani strain by an L1148F substitution in the S2 domain [33]. Hamsters intranasally infected with SARS-CoV-2 were found to resemble human infections by multiple groups [22, 23, 34]. Overall, hamsters intranasally infected with either SARS-CoV or SARS-CoV-2 consistently had similar viral durations and significant pathologies in the lungs. While having similar viral loads and similar duration of viral titres in lungs, GX_P2V(short_3-UTR) in hamsters caused no pathology or clinical signs of disease. We surmise the absence of pathology is likely in part due to the low virulence nature of the GX_P2V spike protein.

Live attenuated vaccines are attractive because they can stimulate a strong and durable immune response with both humoral and cellular immunity. The challenge of constructing live attenuated vaccines is the difficulty of adopting acceptable attenuation strategies. Currently, two live attenuated SARS-CoV-2 vaccine candidates generated by using genome recoding have been reported [35, 36]. The original GX_P2V virus is not a human pathogen, which is advantageous of safety concerns. Our characterization of GX_P2V (short_3UTR) suggests that this variant has a live vaccine potential against SARS-CoV-2 or can be developed as a vaccine vector for the expression of protective antigens like SARS-CoV-2 RBDs. Our data also suggest that shortening the 3'-UTR is a novel strategy for making a live attenuated SARS-CoV-2 variant that warrants further investigations.

Acknowledgements

We thank Harlan D. Caldwell for critical review of the manuscript. The funding sources had no role in the study design, data collection, analysis, interpretation, or writing of the report.

Disclosure statement

No potential conflict of interest was reported by the author (s).

Funding

This research was supported by NSFC-MFST projects (China–Mongolia) [grant numbers 32161143027 and 31961143024], Inner Mongolia Key Research and Development Program [grant number 2019ZD006], Funds for First-class Discipline Construction [grant numbers XK1805 and XK1803-06], National Key Research and Development Program of China [grant numbers 2018YFA0903000, 2020YFC2005405, 2020YFA0712100, 2020YFC0840805, 19SWAQ06, 20SWAQX27 and 20SWAQK22], Fundamental Research Funds for Central Universities [grant numbers BUCTRC201917 and BUCTZY2022], Military Biosecurity Research Program [grant number BWS21J025].

ORCID

Huahao Fan  <http://orcid.org/0000-0001-5007-2158>

Lihua Song  <http://orcid.org/0000-0002-7299-5719>

References

- [1] Zhu N, Zhang D, Wang W, et al. A novel coronavirus from patients with pneumonia in China, 2019. *N Engl J Med.* 2020;382(8):727–733.
- [2] Lu R, Zhao X, Li J, et al. Genomic characterisation and epidemiology of 2019 novel coronavirus: implications for virus origins and receptor binding. *The Lancet.* 2020;395(10224):565–574.
- [3] Wu F, Zhao S, Yu B, et al. A new coronavirus associated with human respiratory disease in China. *Nature.* 2020;579(7798):265–269.
- [4] Zhou P, Yang XL, Wang XG, et al. A pneumonia outbreak associated with a new coronavirus of probable bat origin. *Nature.* 2020;579(7798):270–273.
- [5] Zhou H, Chen X, Hu T, et al. A novel Bat coronavirus closely related to SARS-CoV-2 contains natural insertions at the S1/S2 cleavage site of the spike protein. *Curr Biol.* 2020;30(11):2196–2203.
- [6] Lam TT, Jia N, Zhang YW, et al. Identifying SARS-CoV-2-related coronaviruses in Malayan pangolins. *Nature.* 2020;583(7815):282–285.
- [7] Xiao K, Zhai J, Feng Y, et al. Isolation of SARS-CoV-2-related coronavirus from Malayan pangolins. *Nature.* 2020;583(7815):286–289.
- [8] Murakami S, Kitamura T, Suzuki J, et al. Detection and characterization of Bat sarbecovirus phylogenetically related to SARS-CoV-2, Japan. *Emerg Infect Dis.* 2020;26(12):3025–3029.
- [9] Zhou H, Ji J, Chen X, et al. Identification of novel bat coronaviruses sheds light on the evolutionary origins of SARS-CoV-2 and related viruses. *Cell.* 2021;184(17):4380–4391.
- [10] [Preprint] Sarah T, Khamsing V, Eduard Baquero S, et al. Coronaviruses with a SARS-CoV-2-like receptor-binding domain allowing ACE2-mediated entry into human cells isolated from bats of Indochinese peninsula. *Nature Portfolio.* 2021. doi:10.21203/rs.3.rs-871965/v1
- [11] Zhang S, Qiao S, Yu J, et al. Bat and pangolin coronavirus spike glycoprotein structures provide insights into SARS-CoV-2 evolution. *Nat Commun.* 2021;12(1):1607.
- [12] Chen S, Zhou Y, Chen Y, et al. fastp: an ultra-fast all-in-one FASTQ preprocessor. *Bioinformatics.* 2018;34(17):ii884–iii90.
- [13] Langmead B, Salzberg SL. Fast gapped-read alignment with Bowtie 2. *Nat Methods.* 2012;9(4):357–359.
- [14] Grabherr MG, Haas BJ, Yassour M, et al. Full-length transcriptome assembly from RNA-Seq data without a reference genome. *Nat Biotechnol.* 2011;29(7):644–652.
- [15] Hung JH, Weng Z. Sequence alignment and homology search with BLAST and ClustalW. *Cold Spring Harb Protoc.* 2016;2016(11):10.1101.
- [16] [Preprint] Honko AN, Storm N, Bean DJ, et al. Rapid quantification and neutralization assays for novel coronavirus SARS-CoV-2 using Avicel RC-591 semi-solid overlay. 2020. doi:10.20944/preprints202005.0264.v1
- [17] Seitz M, Beineke A, Seele J, et al. A novel intranasal mouse model for mucosal colonization by

- Streptococcus suis* serotype 2. *J Med Microbiol.* **2012**;61(Pt 9):1311–1318.
- [18] Nie J, Li Q, Wu J, et al. Quantification of SARS-CoV-2 neutralizing antibody by a pseudotyped virus-based assay. *Nat Protoc.* **2020**;15(11):3699–3715.
- [19] Züst R, Miller TB, Goebel SJ, et al. Genetic interactions between an essential 3' cis-acting RNA pseudoknot, replicase gene products, and the extreme 3' End of the mouse coronavirus genome. *J Virol.* **2008**;82(3):1214–1228.
- [20] Kaye M. SARS-associated coronavirus replication in cell lines. *Emerg Infect Dis.* **2006**;12(1):128–133.
- [21] Xie X, Muruato A, Lokugamage KG, et al. An infectious cDNA clone of SARS-CoV-2. *Cell Host Microbe.* **2020**;27(5):841–848.
- [22] Sia SF, Yan L-M, Chin AWH, et al. Pathogenesis and transmission of SARS-CoV-2 in golden hamsters. *Nature.* **2020**;583(7818):834–838.
- [23] Imai M, Iwatsuki-Horimoto K, Hatta M, et al. Syrian hamsters as a small animal model for SARS-CoV-2 infection and countermeasure development. *Proc Natl Acad Sci USA.* **2020**;117(28):16587–16595.
- [24] Chan JF, Zhang AJ, Yuan S, et al. Simulation of the clinical and pathological manifestations of coronavirus disease 2019 (COVID-19) in a golden Syrian hamster model: implications for disease pathogenesis and transmissibility. *Clin Infect Dis.* **2020**;71(9):2428–2446.
- [25] Rokkas T. Gastrointestinal involvement in COVID-19: a systematic review and meta-analysis. *Ann Gastroenterol.* **2020**;33(4):355–365.
- [26] Lee AC, Zhang AJ, Chan JF, et al. Oral SARS-CoV-2 inoculation establishes subclinical respiratory infection with virus shedding in golden Syrian hamsters. *Cell Rep Med.* **2020**;1(7):100121.
- [27] Zhang Y, Huang K, Wang T, et al. SARS-CoV-2 rapidly adapts in aged BALB/c mice and induces typical pneumonia. *J Virol.* **2021**;95(11):e02477-20.
- [28] Gu H, Chen Q, Yang G, et al. Adaptation of SARS-CoV-2 in BALB/c mice for testing vaccine efficacy. *Science.* **2020**;369(6511):1603–1607.
- [29] Ogando NS, Dalebout TJ, Zevenhoven-Dobbe JC, et al. SARS-coronavirus-2 replication in vero E6 cells: replication kinetics, rapid adaptation and cytopathology. *J Gen Virol.* **2020**;101(9):925–940.
- [30] Goebel SJ, Miller TB, Bennett CJ, et al. A hypervariable region within the 3' cis-acting element of the murine coronavirus genome is nonessential for RNA synthesis but affects pathogenesis. *J Virol.* **2007**;81(3):1274–1287.
- [31] Goh GK, Dunker AK, Foster JA, et al. Shell disorder analysis suggests that pangolins offered a window for a silent spread of an attenuated SARS-CoV-2 precursor among humans. *J Proteome Res.* **2020**;19(11):4543–4552.
- [32] Roberts A, Vogel L, Guarner J, et al. Severe acute respiratory syndrome coronavirus infection of golden Syrian hamsters. *J Virol.* **2005**;79(1):503–511.
- [33] Roberts A, Lamirande EW, Vogel L, et al. Animal models and vaccines for SARS-CoV infection. *Virus Res.* **2008**;133(1):20–32.
- [34] Song Z, Bao L, Yu P, et al. SARS-CoV-2 causes a systemically multiple organs damages and dissemination in hamsters. *Front Microbiol.* **2021**;11:618891.
- [35] Wang Y, Yang C, Song Y, et al. Scalable live-attenuated SARS-CoV-2 vaccine candidate demonstrates preclinical safety and efficacy. *Proc Natl Acad Sci USA.* **2021**;118(29):e2102775118.
- [36] Trimpert J, Dietert K, Firsching TC, et al. Development of safe and highly protective live-attenuated SARS-CoV-2 vaccine candidates by genome recoding. *Cell Rep.* **2021**;36(5):109493.